Performance Evaluation for Frequency Response Services from Miscellaneous Energy Resources

Jianguo Zhou, Ye Guo*, *Senior Member, IEEE,* Hanyang Lin, Yinliang Xu, *Senior Member, IEEE,* Lun Yang, Jinghan He, *Fellow, IEEE,* Hongbin Sun, *Fellow, IEEE*

***Abstract*—The phase out of conventional synchronous generators (SGs) and vigorous development of renewable energy sources (RESs) is indisputably leading to a significant reduction in inertia of power grids, blowing a hole in frequency security and stability. To address this issue, various fast-acting resources such as battery energy systems (BESS) are being discussed worldwide. Accurate quantifying the relative effectiveness of these resources in arresting frequency decline to conventional methods is, therefore, of great significance to securely operate low-inertia power systems (LIPS). To do so, an analytical model of Equivalent Frequency-Containment Performance Ratio (EFCPR) is proposed for heterogeneous resources having different response characteristics. Furthermore, two Sigmoid-function-based approaches are also proposed to extend the EFCPR model to aggregated resources, and a more general scenario taking delivery time instant of instantaneous response BESS into account. Numerical results on the Texas test case and the Great Britain power grids with real operation data (from September 2023 to December 2024) collected from the National Energy System Operator (NESO) websites validate the EFCPR model and penetrate many of parameters' impacts.**

***Index Terms*—Frequency control, Frequency response, Frequency stability, Energy resources**

NOMENCLATURE

General Notation

$\boldsymbol{v}^\top$	Transpose of a general vector or matrix $\boldsymbol{v}$
$\mathbf{1}$	Vector of ones with appropriate dimensions
$\mathcal{G}, \mathcal{B}, \mathcal{V}$	Set of resources providing $\boldsymbol{r}$, $\boldsymbol{b}$ and $\boldsymbol{v}$, respectively.
$\mid \mathcal{B} \mid$	Number of resources in $\mathcal{B}$
$\mid \mathcal{G} \mid$	Number of resources in $\mathcal{G}$
$\mid \mathcal{V} \mid$	Number of resources in $\mathcal{V}$
v_i	Element i of a general vector $\boldsymbol{v}$

Parameters and Variables

$\alpha(\cdot), \boldsymbol{\beta(\cdot)}$	The EFCPR of $\boldsymbol{b}$ and $\boldsymbol{v}$, respectively
$\boldsymbol{\nu}(\cdot)$	Frequency response reserve demand
$\boldsymbol{b}$	Service volume provided by sources that can instantaneously deliver expected power
$\boldsymbol{R}$	Primary frequency control reserve provided by SGs
$\boldsymbol{v}$	Service volume provided by VRE resources
$\widehat{K}_{\text{min}}$	The minimum ramp rate considering aggregated resources
f_0	The nominal frequency of the system in [Hz]
f_{db}	The dead-band frequency
f_{min}	The minimum system frequency
f_{nad}	The system nadir frequency
H	Total system inertia in [GWs]
K_{min}	The minimum ramp rate
L	Power loss
r_g	Delivered volume of PFR from SG g
T_{agg}	The overall delivery time of aggregated resources
$t_{\text{d,agg}}$	The overall delay time of aggregated resources
t_{nad}	The time when frequency reaches the nadir value
t_{db}	The time of dead band
t_d	The delay time
T_g	The delivery time of PFR r_g
T_j	The delivery time of the service v_j
V_{agg}	The total volume provided by aggregated resources
ζ	The system damping and frequency responsive load

This work was supported by the National Natural Science Foundation of China under Grant (52377105, 52307138). (*Corresponding Author: Ye Guo*)

J. Zhou and J. He are with the Energy and Electricity Research Center, International Energy College, Jinan University (Zhuhai), 519070 Zhuhai, Guangdong, P. R. China. (jgzhou@jnu.edu.cn; hejinghan@jnu.edu.cn).

Y. Guo is with the Department of Building Environment and Energy Engineering, the Hong Kong Polytechnic University, Hong Kong, P.R. China. (ye.guo@polyu.edu.hk)

Y. Xu and H. Lin are with the Tsinghua Shenzhen International Graduate School, Tsinghua University, 518055 Shenzhen, Guangdong, P. R. China. (xu.yinliang@sz.tsinghua.edu.cn; linhy22@mails.tsinghua.edu.cn).

L. Yang is with the School of Automation Science and Engineering, Xi'an Jiaotong University, Xi'an, Shaanxi 710049 China. (yanglun@xjtu.edu.cn)

H. Sun is with the Department of Electrical Engineering, State Key Laboratory of Power Systems, Tsinghua University, 100084 Beijing, P. R. China. (email: shb@tsinghua.edu.cn).

I. INTRODUCTION

A. Background

THe phase out of conventional synchronous generators (SGs) and vigorous development of renewable energy sources (RESs) along with the increasing High Voltage Direct Current (HVDC) including Multi-Terminal HVDC links is leading to a significant reduction in inertia of power grids. For instance, the system inertia of Great Britain (GB) power grid could be reduced by up to about 70% in 2033/34 [1]), Texas in the United States reached at 109 GWs with a 100 GWs critical inertia on March 22, 2021 [2], and (potential) inertia shortfall in South Australia and Tasmania [3]. This reduction is in turn blowing a hole in frequency security and stability [4]. For instance, the blackout of the Southern Australia grid in September 2016 (wind power generation accounted for 48% before the event), after which the frequency dropped from 49.5 Hz to 47 Hz in 0.4s, and the rate of change of frequency (RoCoF) was as high as 6.25 Hz/s, exceeding the system's ability to maintain stability [5]. Similar issues can also be found in some other events in Australia during 2018-2020 [6], [7], GB in 2019 [8], and the Continental European Area in 2021 [9], and happen more frequently in recent years.

To achieve proper frequency control (keep frequency nadir, RoCoF, and quasi-steady-state frequency within permitted ranges), various fast-acting resources, which can provide Fast Frequency Response (FFR) services (much faster than primary frequency response (PFR)), such as battery energy systems (BESS), wind farms (WFs), and HVDC links, are being discussed worldwide and have been regarded as promising options. However, how to accurately or analytically quantify

their relative effectiveness in frequency control compared to conventional methods is still a main research gap, which is a challenging problem and of great significance for system operators to securely and economically operate low-inertia power systems (LIPS). Resources may have different characteristics such as response rate, sustainable time, and support capacity, meaning different effectiveness or performance in frequency containment. In the LIPS, the system frequency changes more dramatically and rapidly after a large disturbance occurs, requiring faster and more accurate support. Over-estimation of effectiveness will lead to insufficient frequency response reserve, resulting in insecure system operation. Conversely, underestimation of effectiveness will lead to redundant frequency response reserve, resulting in higher reserve costs. Furthermore, accurately quantifying the relative effectiveness can enable more reasonable pricing for the FFR, incentivizing their participation in the market.

B. Literature Review

Currently, incorporating the Frequency Security Constraints (FSCs) including frequency nadir (Δf_{nad}), RoCoF and quasi-steady-state frequency (Δf_{qss}) into the optimization model is a common practice to maintain the frequency within acceptable limits. RESs based on converters [10] such as WFs [1], [11]–[15] and PV [16], ESS systems [13], [17]–[21], [27], MTDC-connected WFs [26], [33], HVDC-connected systems [31], [32], and load [22], [23] are investigated for providing VIR, FFR, or both due to their fast response strength that conventional SGs cannot match. To take the heterogeneous temporal-spatial distribution of inertia, PFR, and FFR resources into account, distinct frequency dynamics and mutual frequency support between areas also have been studied recently [27]–[33]. The above works are mainly dedicated to addressing two important issues, namely, modeling FSCs and modeling uncertainties. Two categories of approaches, analytical methods and data-driven methods, are primarily adopted to establish the FSCs. Methods from PWL [11], [18] to bound extraction [10], and big-M methods [14], [15], [20], [21] are mainly used to process the high nonlinear and nonconvex analytical FSCs where dynamics [10], [11], response speed [20], [21], [24], dead-band [14], [15] of PFR/FFR and IR/VIR, and fixed/variable droop and ineria [19] are usually taken into account. Recently, data-driven methods such as deep neural networks (DNN) [25] and linear regressions [30] have been proposed to model FSCs. Uncertainty modeling is an extremely significant work in the LIPS operation. Scenario-based stochastic programming [1], [10], [20], robust optimization [12], interval-based optimization [26], and distributionally robust chance-constrained optimization [14], [15] have been widely reported.

These prior-art works have offered significant contributions to frequency security. However, most of them do not well distinguish the effectiveness of resources providing different types of services. To quantify the effectiveness, the concept of equivalency ratios has been proposed in [36], [37] where the ratio values are empirically determined via simulating the Electric Reliability Council of Texas (ERCOT) system when deriving the frequency control reserve requirement, and the weighted sum of PFR and FFR reserve are larger than an empirically found requirement quantity. On February 3, 2025, ERCOT Board was expected to endorse for Public Utility Commission of Texas (PUCT) approval of the updated 2025 ERCOT's methodology for determining minimum Ancillary Service Requirements [38], where the equivalency ratio between load resources and generation resources will be used to determine the responsive reserve requirement. To analytically describe the relative effectiveness, Manuel Garcia et al [39] proposed an equivalency ratio model from first principles to form the PFR reserve limit and study the co-optimization problem based on their previous works [40], [41]. The results closely match the empirical data from [36], [37]. Another performance ratio was derived by integrating the dynamics of frequency deviation [42], where the results show that the performance ratio increases with the increase of system inertia, which is inconsistent with those obtained in [36], [37], [39] and general industrial experience. Similar to the equivalency ratio, the concept of exchange rates was proposed by NESO who recently published the exchange rate values for dynamic services (DC, DM, and DR) [54]. However, how to determine the exchange rates is still an open question. Additionally, the coefficients in the constraints presented in [29], [30] and our previous work [43] are essentially the quantification of the relative effectiveness of frequency response services that have distinct characteristics. Unfortunately, these results are still numerically obtained, requiring a large number of simulations.

Despite the significant advancement of the aforementioned works, there are still some major gaps to be addressed. First of all, existing works mainly focus on deriving the equivalency ratio between two types of services (FFR and PFR). If the third type of responsive service is included, it is still unknown that what the equivalency ratio will be and that how to distinguish the difference between FFR and the third type of responsive service. Another critical concern is that how to measure the overall effectiveness of aggregated resources if considered and how to differentiate the effectiveness of various aggregators. Finally, how does the triggering time instant of the service that can instantaneously deliver expected power impact the performance? These issues have not been studied yet.

C. Contributions and Organization

To fill the gaps, this paper focuses on the modeling of performance in providing frequency response services for heterogeneous resources, aiming at accurately quantifying their relative effectiveness to conventional SGs. The main contributions are summarized as follows.

(1) An analytical model, Equivalent Frequency-Containment Performance Ratio (EFCPR), is proposed for heterogeneous resources that have different response characteristics, which can explicitly capture interactions of frequency response services and impacts of parameters on the EFCPR values.

(2) Two Sigmoid-function-based approaches are further proposed to extend the EFCPR model to aggregated resources and a more general scenario considering delivery-time instant of BESS that can instantaneously release the expected energy, which can differentiate frequency response services from aggregated resources and have not been explored previously.

(3) Numerical studies using both the modified GB power grids with latest real operational data collected from the NESO websites for over a year (Sept. 2023 - Dec. 2024) and the Texas test case are carried out. The results perfectly match both the empirical operation data from ERCOT and the exchange rate published by NESO, demonstrating the effectiveness of the proposed model and penetrating many of parameters' impacts.

The rest of the paper is organized as follows. Section II establishes the model of the EFCPR and its extension to more general scenarios. Section III presents the numerical results to validate the proposed model. Section IV provides some discussions. Conclusions are finally drawn in Section V.

II. Modeling of The EFCPR

A. Assumptions and Definition

Some assumptions and definitions are presented before going into detailed modeling of the EFCPR. These assumptions are general and widely used in existing works.

***Assumption* 1.** *(1) The frequency control reserve provided by fast-acting resources can be fully deployed and can meet the duration requirement. The deployed volume r_g is realized via SG's droop control and should not exceed the procured reserve for primary frequency control, i.e., $r_g \le R_g, \forall g \in \mathcal{G}$. (2) We assume that the power responses of resource providing v_j and r_g are modeled as a linear ramp, and the time delays of all resources are set as the same value of t_d. It is a common practice to make this assumption, which is in line with existing works such as [14], [15], [20], [21], [24], [39]–[41]. (3) The BESS can provide the amount of power $\boldsymbol{b}$ instantaneously. The deployment of the frequency control reserve occurs during the ramping of SGs. There is sufficient reserve to restore power balance and the power imbalance remains non-positive immediately after the reserve is deployed. (4) It is assumed that the data of parameters about all resources used for the calculation of the EFCPR such as response times and ramp rates submitted by service providers are available for system operators, which is in line with some existing published works.*

***Definition* 1.** *EFCPRs are the coefficients describing the relative effectiveness of FFR reserves provided by distinct fast-acting resources to PFR reserves in frequency control. This can be interpreted as: FFR is $\alpha(\cdot)$ ($\boldsymbol{\beta}(\cdot)$, see Eq. (1)) times as effective as PFR in decreasing the frequency deviation.*

Now we are ready to model the EFCPRs. Consider a LIPS, the reserve requirement of primary frequency control can be generalized as follows:

$$\mathbf{1}^\top \boldsymbol{R} + \alpha(\cdot)\mathbf{1}^\top \boldsymbol{b} + \boldsymbol{\beta}(\cdot)^\top \boldsymbol{v} \ge \nu(\cdot) \tag{1}$$

where $\boldsymbol{R} = [R_1, \cdots, R_{|\mathcal{G}|}]^\top$ is the primary frequency control reserve provided by SGs, $\boldsymbol{b} = [b_1, \cdots, b_{|\mathcal{B}|}]^\top$ is the service volume provided by sources that can instantaneously deliver expected power such as BESS, and $\boldsymbol{v} = [v_1, \cdots, v_{|\mathcal{V}|}]^\top$ is the amount of the third type of service provided by variable renewable energy (VRE) resources (aggregators) with different characteristics such as WTG/PVG and virtual power plant. $\nu(\cdot)$ is the reserve demand, and $\alpha(\cdot)$ and $\boldsymbol{\beta}(\cdot) = [\beta_1(\cdot), \cdots, \beta_{|\mathcal{V}|}(\cdot)]$ are the EFCPR of $\boldsymbol{b}$ and $\boldsymbol{v}$, respectively. $|\mathcal{G}|$, $|\mathcal{B}|$ and $|\mathcal{V}|$ are the number of resources providing $\boldsymbol{r}$, $\boldsymbol{b}$ and $\boldsymbol{v}$, respectively. r_g, b_i, and v_j are used to denote the deployed primary frequency control reserve provided by source g, i and j, respectively.

To derive the EFCPR, i.e., $\alpha(\cdot)$ and $\boldsymbol{\beta}(\cdot)$, we start from the system frequency response dynamics under the power loss of L, which is depicted in Fig. 1. The frequency dynamics can be simplified as the well-known swing equation (2) [20], [21]:

$$2H/f_0 \dot{f}(t) = \mathbf{1}^\top \overrightarrow{\boldsymbol{r}}(t) + \mathbf{1}^\top \overrightarrow{\boldsymbol{b}}(t) + \mathbf{1}^\top \overrightarrow{\boldsymbol{v}}(t) - L \tag{2}$$

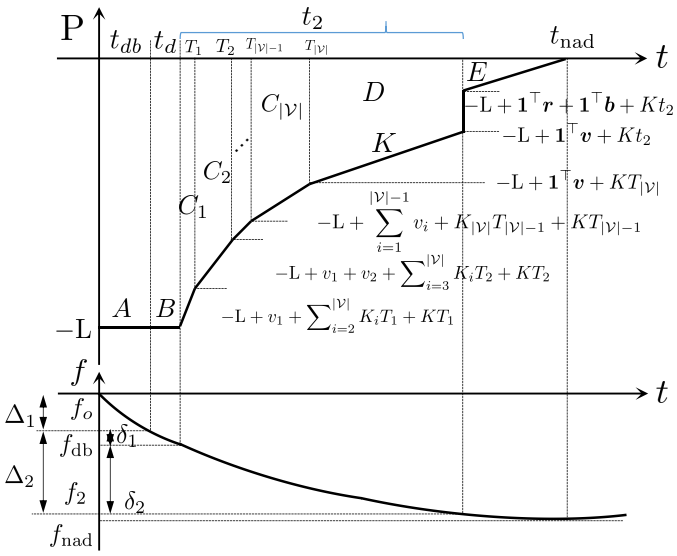

Fig. 1. Response trajectories of power and frequency under the loss of L.

where f_0 is the nominal frequency, and H is the total system inertia. In this paper, virtual inertia provided by these fast-acting resources is also considered and has been included in H. The power $\overrightarrow{\boldsymbol{r}}(t)$, $\overrightarrow{\boldsymbol{b}}(t)$, and $\overrightarrow{\boldsymbol{v}}(t)$ are, respectively, described as (3), (4) and (5).

$$\overrightarrow{\boldsymbol{r}}(t) = \begin{cases} \mathbf{0} & t \le t_{db} + t_d \\ \frac{\boldsymbol{r}}{T_g}(t - t_{db} - t_d) & t_{db} + t_d < t \le t_{db} + t_d + T_g \\ \boldsymbol{r} & t > t_{db} + t_d + T_g \end{cases} \tag{3}$$

$$\overrightarrow{\boldsymbol{b}}(t) = \begin{cases} \mathbf{0} & t \le t_{db} + t_d + t_2 \\ \boldsymbol{b} & t > t_{db} + t_d + t_2 \end{cases} \tag{4}$$

where $\boldsymbol{K}^\top = \left[\frac{v_1}{T_1}, \frac{v_2}{T_2}, \cdots, \frac{v_{|\mathcal{V}|}}{T_{|\mathcal{V}|}}\right]$, T_g is the delivery time.

B. BESS Deployed after all VREs Deployed

For convenience, we start from the scenario that the service $\boldsymbol{b}$ is delivered after the services $\boldsymbol{v}$ have been delivered. It is not difficult to observe that the nadir frequency f_{nad} will increase if the ramp rate K is increased (In fact, as shown in Fig. 1 and (A7) given in Appendix, f_{nad} is strictly monotonically increasing with K). Therefore, there is a minimum ramp rate $K_{\min}$ such that $f_{\text{nad}} = f_{\min}$, and $f_{\text{nad}} \ge f_{\min}$ can be guaranteed if $K \ge K_{\min}$. Combine (2) - (5) and Fig. 1, the minimum ramp rate of SGs to satisfy the minimum frequency requirement considering services $\boldsymbol{b}$ and $\boldsymbol{v}$ can be derived and given by (6) through a series of mathematical operations attached in Appendix, where $\boldsymbol{T}^\top = \left[T_1, T_2, \cdots, T_{|\mathcal{V}|}\right]$, $\Delta_1 = f_0 - f_{\text{db}}$ is the frequency deviation between the rated frequency f_0 and the dead-band frequency f_{db}, $\Delta_2 = f_{\text{db}} - f_2$ is the deviation between the dead-band frequency f_{db} and the frequency f_2 at which $\boldsymbol{b}$ is deployed, and $\Delta_3 = f_0 - f_{\text{nad}} - \Delta_1 - \Delta_2$ is the frequency deviation between the frequency f_2 and the nadir frequency f_{nad}. Actually, $\boldsymbol{b}$ and $\boldsymbol{v}$ equal to their frequency control reserve, respectively, according to the Assumption 1.

Further, if all the generators with ramp rate K_g, $g \in \mathcal{G}$ can deploy the primary frequency control reserve by the time $t_{\min}$ corresponding to the minimum ramp rate $K_{\min}$, i.e.,

$$r_g \le K_g(t_{\min} - t_{\text{db}} - t_{\text{d}}), \tag{7}$$

$$\mathbf{1}^\top \overrightarrow{\boldsymbol{v}}(t) = \begin{cases} 0 & t \le t_{db} + t_d \\ \mathbf{1}^\top \boldsymbol{K} \cdot (t - t_{db} - t_d) & t_{db} + t_d < t \le t_{db} + t_d + T_1 \\ v_1 + \sum_{j=2}^{|\mathcal{V}|} \frac{v_j}{T_j} \cdot (t - t_{db} - t_d) & t_{db} + t_d + T_1 < t \le t_{db} + t_d + T_2 \\ \cdots & \cdots \\ \sum_{j=1}^{|\mathcal{V}|-1} v_j + \frac{v_{|\mathcal{V}|}}{T_{|\mathcal{V}|}} \cdot (t - t_{db} - t_d) & t_{db} + t_d + T_{|\mathcal{V}|-1} < t \le t_{db} + t_d + T_{|\mathcal{V}|} \\ \mathbf{1}^\top \boldsymbol{v} & t > t_{db} + t_d + T_{|\mathcal{V}|} \end{cases} \tag{5}$$

$$K_{\min} = \frac{\left\{ \mathbf{1}^\top \boldsymbol{b} \sqrt{\Delta_3} - \sqrt{\left[\Delta_2 + \Delta_3 - \frac{f_0}{2H} \left(L t_d + \frac{1}{2} \boldsymbol{T}^\top \boldsymbol{v} \right) \right] (L - \mathbf{1}^\top \boldsymbol{v})^2 - \left[\Delta_2 - \frac{f_0}{2H} \left(L t_d + \frac{1}{2} \boldsymbol{T}^\top \boldsymbol{v} \right) \right] (\mathbf{1}^\top \boldsymbol{b})^2} \right\}^2}{\frac{4H}{f_0} \left[\Delta_2 + \Delta_3 - \frac{f_0}{2H} \left(L t_d + \frac{1}{2} \boldsymbol{T}^\top \boldsymbol{v} \right) \right]^2} \tag{6}$$

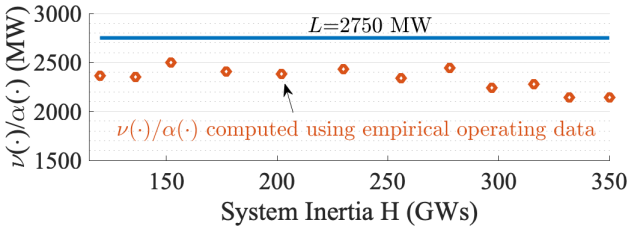

Fig. 2. Profile of $\nu(\cdot)/\alpha(\cdot)$ across different system inertia levels.

then, the nadir frequency requirement $f_{\text{nad}} \ge f_{\min}$ can be guaranteed. $T_{\max}(L, H, \boldsymbol{v}, \boldsymbol{b}, \boldsymbol{\Delta}, \boldsymbol{T}, t_d) = t_{\min} - t_{\text{db}} - t_{\text{d}}$, which can be interpreted as the slowest ramp time requirement for SGs, is given by

$$T_{\max}(L, H, \boldsymbol{v}, \boldsymbol{b}, \boldsymbol{\Delta}, \boldsymbol{T}, t_d) = (L - \mathbf{1}^\top \boldsymbol{v} - \mathbf{1}^\top \boldsymbol{b}) / K_{\min} \tag{8}$$

where $\boldsymbol{\Delta} = [\Delta_1, \Delta_2, \Delta_3]^\top$.

For generators, we assume that the delivered primary frequency control reserve r_g equals to the reference mechanical power of the turbine governor provided via droop control, i.e., $r_g = \xi_g (\Delta f - \Delta_1)$, where ξ_g is the droop coefficient. Then, when the frequency reaches f_{nad}, the value of r_{g} will be $r_{\text{g}}^{\text{nad}} = \xi_g (\Delta f_{\text{nad}} - \Delta_1)$. Generally, for the sake of security and stability, the delivered power r_g should be proportional to the headroom of the generator, and intuitively, any primary frequency control reserve R_g that exceeds the amount $\xi_g (\Delta f_{\text{nad}} - \Delta_1)$ will not be utilized to support frequency response. Therefore, we roughly make $\xi_g (\Delta f_{\text{nad}} - \Delta_1)$ equal to R_g, i.e., $\xi_g (\Delta f_{\text{nad}} - \Delta_1) \approx R_g$. Then, the following equation can be derived:

$$K_g = \frac{\xi_g (\Delta f_{\text{nad}} - \Delta_1)}{t_{\text{nad}} - t_{\text{db}} - t_{\text{d}}} = \frac{1}{t_{\text{nad}} - t_{\text{db}} - t_{\text{d}}} R_g \tag{9}$$

where t_{nad}, the time when frequency drops to f_{nad}, can be calculated directly using (2), and can be expressed as (10).

$$t_{\text{nad}} = \frac{(L - \mathbf{1}^\top \boldsymbol{b} - \mathbf{1}^\top \boldsymbol{v}) T_g}{\mathbf{1}^\top \boldsymbol{r}} + t_{\text{db}} + t_{\text{d}} \tag{10}$$

Then, (7) can be rewritten as

$$r_g \le \frac{L - \mathbf{1}^\top \boldsymbol{v} - \mathbf{1}^\top \boldsymbol{b}}{(t_{\text{nad}} - t_{\text{db}} - t_{\text{d}}) K_{\min}} R_g. \tag{11}$$

Note that Fig. 2 obtained using the data presented in the literature [36], [37] shows that the ratio $\nu(\cdot)/\alpha(\cdot)$ is almost constant no matter how the inertia changes, and slightly less than the power loss L. The slight fluctuation may be caused by system noise. System damping and frequency responsive load, represented by ζ, may contribute to this slight mismatch. With the above consideration, it is assumed that $\nu(\cdot)$ is approximately equal to $\alpha(\cdot)(L + \boldsymbol{\zeta})$, i.e., $\nu(\cdot) \approx \alpha(\cdot)(L + \boldsymbol{\zeta})$. Additionally, this assumption has also been utilized in the literature [39], [41]. Consequently, the requirement (1) can be rewritten as

$$\frac{1}{\alpha(\cdot)} \mathbf{1}^\top \boldsymbol{R} + \mathbf{1}^\top \boldsymbol{b} + \frac{1}{\alpha(\cdot)} \boldsymbol{\beta}(\cdot)^\top \boldsymbol{v} \ge L + \boldsymbol{\zeta}. \tag{12}$$

We believe that the main performance difference between BESS and VREs in providing primary frequency control could be intimately bound up with the response time and response rate, i.e., T_j and $K_j, j \in \mathcal{V}$ (For aggregated resources, it could be the overall response time and the placement of resources within the aggregators. This has been further discussed in Section III-B). Intuitively, the performance will deteriorate as the response time increases. With this in mind, $\boldsymbol{\beta}(\cdot)$ could be approximated as $\boldsymbol{\varphi}(\boldsymbol{T}, \boldsymbol{K})\alpha(\cdot)$. Then, (12) can be written as

$$\frac{1}{\alpha(\cdot)} \mathbf{1}^\top \boldsymbol{R} + \mathbf{1}^\top \boldsymbol{b} + \boldsymbol{\varphi}(\boldsymbol{T}, \boldsymbol{K})^\top \boldsymbol{v} \ge L + \boldsymbol{\zeta} \tag{13}$$

where $\boldsymbol{\varphi}(\boldsymbol{T}, \boldsymbol{K})^\top = \left[\varphi_1(T_1, K_1), \cdots, \varphi_{|\mathcal{V}|}(T_{|\mathcal{V}|}, K_{|\mathcal{V}|})\right]$ in which $\varphi_j(T_j, K_j)$ is described as $\varphi_j(T_j, K_j) = K_j / (a_j T_j + 1), j \in \mathcal{V}$. This constraint (13) holds if and only if (14) and (15) hold.

$$\mathbf{1}^\top \boldsymbol{r} + \mathbf{1}^\top \boldsymbol{b} + \boldsymbol{\varphi}(\boldsymbol{T}, \boldsymbol{K})^\top \boldsymbol{v} \ge L + \boldsymbol{\zeta} \tag{14}$$

$$\boldsymbol{r} \le \boldsymbol{R} / \alpha(\cdot) \tag{15}$$

Generally, researchers and operators are likely to have a common view that BESS and VREs could perform better than SGs in frequency support, especially in low-inertia power systems. Therefore, by comparing (15) with (11), the EFCPR, $\alpha(\cdot)$ and $\boldsymbol{\beta}(\cdot)$, can be approximately modeled as follows, respectively:

$$\alpha(\cdot) = \max\left\{1, \frac{(t_{\text{nad}} - t_{\text{db}} - t_{\text{d}}) K_{\min}}{L - \mathbf{1}^\top \boldsymbol{v} - \mathbf{1}^\top \boldsymbol{b}}\right\} \tag{16}$$

$$\boldsymbol{\beta}(\cdot) = \max\left\{1, \boldsymbol{\varphi}(\boldsymbol{T}, \boldsymbol{K})\alpha(\cdot)\right\} \tag{17}$$

where $t_{\text{db}} = 2H\Delta_1 / L f_0$, $t_{\text{d}} = 2H\delta_1 / L f_0$.

C. BESS Deployed Between T_{n-1} and T_n

In this subsection, we further extend the results obtained in the above subsection to a more generalized scenario that the service $\boldsymbol{b}$ is delivered between T_{n-1} and T_n, $1 \leq n \leq |\ \mathcal{V}\ |$. That is to say, BESS delivers the power after the $(n-1)$th resource fully delivered the reserve but before the nth one.

With a similar process, the time t_2 can be derived as

$$t_2 = \frac{1}{K+K_{\mathrm{V}}}\left(\widetilde{L} - \sqrt{\widetilde{L}^2 - \frac{4H}{f_0}\left(K+K_{\mathrm{V}}\right)\widetilde{\delta}_2}\right) \tag{18}$$

where $K_{\mathrm{V}} = \sum_{j=n}^{\mathcal{V}} \frac{v_j}{T_j}$, $\widetilde{L} = L - \sum_{i=1}^{n-1} v_i$, and $\widetilde{\delta}_2 = \delta_2 - \frac{f_0}{4H}\sum_{i=1}^{n-1} v_i T_i$. After a series of mathematical operations, the same equation as (A7) can be established in this general scenario. Then the ramp rate K will be derived by solving equation (19) which is a four-order equation caused by K_{V} in (19). Equation (19), where $\widehat{L} = \left(L - \mathbf{1}^\top \boldsymbol{v} - \mathbf{1}^\top \boldsymbol{b}\right)^2 + 2\left(\mathbf{1}^\top \boldsymbol{b}\right)\widetilde{L}$, could have four solutions. According to the engineering practice, the minimum ramp rate denoted $K_{\min}$ can exist, and can be obtained by using Lodovico Ferrari method and computer. Then, the equivalent ratios denoted $\widetilde{\alpha}(\cdot)$ and $\widetilde{\boldsymbol{\beta}}(\cdot)$ can be given by (20) and (21), respectively.

$$\widetilde{\alpha}(\cdot) = \max\left\{1, \frac{\left(t_{\mathrm{nad}} - t_{\mathrm{db}} - t_{\mathrm{d}}\right)\widetilde{K}_{\min}}{L - \mathbf{1}^\top \boldsymbol{v} - \mathbf{1}^\top \boldsymbol{b}}\right\}, \tag{20}$$

$$\widetilde{\boldsymbol{\beta}}(\cdot) = \max\left\{1, \boldsymbol{\varphi}(\boldsymbol{T}, \boldsymbol{K})\widetilde{\alpha}(\cdot)\right\}. \tag{21}$$

***Remark* 1.** *The proposed model has some salient features:*

1) It analytically describes the impacts and interactions of various parameters/variables including those of the system and individual service on the EFCPR values.

2) The developed model (9) establishes the proportional relationship between the ramp rate of SGs K_g and the procured primary frequency control reserve R_g. It is the time instant at the nadir frequency t_{nad} along with dead-band time t_{db} and response time delay t_d that this proportion is closely related to. The time t_{nad} shown in (10) depends on many variable parameters. This means that the proportion is not a constant.

3) Both $\boldsymbol{b}$ and $\boldsymbol{v}$ provided by resources (and/or aggregators) with distinct response characteristics are considered in the model thereby distinguishing ratios of different resources and analyzing the impacts of various parameters and services on the ratios. It is observed that a resource with a smaller delivery time has a higher equivalent ratio, which means it has better performance and this is in line with the intuition.

4) The models (20) and (21) are more general, and have the ability to describe the influence of the time instants when the reserve $\boldsymbol{b}$ is instantaneously delivered. Essentially, the minimum ramp rate K_{min} in (6) is a special case of $\widetilde{K}_{min}$ obtained by solving (19) since if $\boldsymbol{b}$ is delivered after all $\boldsymbol{v}$ have been fully delivered, the parameter K_V will be zero and (19) becomes (A8). Consequently, it will result in $\widetilde{K}_{min} = K_{min}$. Further, K_V will reach its maximum value when $\boldsymbol{b}$ is delivered at the time of $t_{db}+t_d$. This is also a special case of the models (20) and (21).

5) Inverter-based resources can also provide inertia support. The proposed modeling method can be extended to evaluate the inertia response performance by rearranging (1) as $\mathbf{1}^\top \boldsymbol{R} + \alpha(\cdot)\left(\mathbf{1}^\top \boldsymbol{b}\right) + \boldsymbol{\beta}(\cdot)^\top \left[\boldsymbol{v}^\top, \left(\mathbf{1}^\top \boldsymbol{h}_I\right)\right]^\top \geq \nu(\cdot)$ and (2) as $2H/f_0 \dot{f}(t) = \mathbf{1}^\top \overrightarrow{\boldsymbol{r}}(t) + \mathbf{1}^\top \overrightarrow{\boldsymbol{b}}(t) + \mathbf{1}^\top \overrightarrow{\boldsymbol{v}}(t) + \mathbf{1}^\top \overrightarrow{\boldsymbol{h}}(t) - L$, where the inertia response reserve $\boldsymbol{h}_I$ from inverters is regarded as a supper fast response service. The main difficulty could be the overall approximate PWL inertia response characteristics $\overrightarrow{\boldsymbol{h}}(t)$ similar to that in (5), and that inertia response can be sustained for a very short period of time only, which is different from the FFR and PFR, making the deriving more challenging.

D. Sigmoid-based Extension to Aggregated Resources

The above two subsections discussed the EFCPR modeling for resources providing a single type of service $\boldsymbol{b}$ or $\boldsymbol{v}$. A natural question is what the overall EFCPR of the aggregated resources such as virtual power plants and co-located power plants will be if they would like to simultaneously provide different types of services such as FFR, PFR, and even Static Firm Frequency Response (SFFR) in the market. By doing so, there could be at least two potential benefits, i.e., attracting more resources to participate in the market and reducing the scale of optimization models. This is also motivated by some grid-code specifications for dynamical frequency regulation in which a normalized active power capacity to be delivered with a delay time, a delivery time, and duration time, and/or a specified frequency deviation is usually defined. Some examples are Fast Frequency Response in Nordic area [44], RRS service (include FFR, PFR, Load Resource) in ERCOT [45], DC/DM/DR services in NESO [46], and some files in China [47]. These grid codes generally present prescribed piece-wise linear time-domain response characteristics, resulting in different response rates in different periods. This can be illustrated by using the example shown in Fig. 3, where four different sub-type products for frequency response with different time delays and full response times are denoted by four thin red solid lines, respectively, and the thick red solid line displays the corresponding response characteristic of the aggregated services $\mathbf{1}^\top \boldsymbol{v}$. This subsection aims to model the EFCPR of the aggregated services rather than a single type within the aggregator. $v_{\mathrm{agg}}(t)$ is used to represent the aggregated frequency response dynamics. Then, the time t_2 can be derived by taking steps similar to the previous subsections:

$$t_2 = \frac{1}{K}\left(\overline{L} - \sqrt{\overline{L}^2 - \frac{4H}{f_0}K\widehat{\delta}_2}\right) \tag{22}$$

where $\widehat{\delta}_2 = \delta_2 - \frac{f_0}{2H}\left[T_{\mathrm{agg}}V_{\mathrm{agg}} - S_{\mathrm{agg}}\right]$, and $S_{\mathrm{agg}} = \int_{t_{\mathrm{db}}+t_{\mathrm{d}}}^{T_{\mathrm{agg}}+t_{\mathrm{db}}+t_{\mathrm{d}}} v_{\mathrm{agg}}(t)\,dt$, $V_{\mathrm{agg}} = \lim_{t \to T_{\mathrm{agg}}} v_{\mathrm{agg}}(t) = \mathbf{1}^\top \boldsymbol{v}$. The minimum ramp rate requirement denoted by $\widehat{K}_{\min}$ can be given by (23) via solving the equation

$$\begin{aligned}\left[\frac{2H}{f_0}\varpi - \left(T_{\mathrm{agg}}V_{\mathrm{agg}} - S_{\mathrm{agg}}\right)\right]^2 K^2 + \Big[\left(T_{\mathrm{agg}}V_{\mathrm{agg}} - S_{\mathrm{agg}}\right.\\ \left. - \frac{2H}{f_0}\varpi\right)\left(\overline{L}^2 + \left(\mathbf{1}^\top \boldsymbol{b}\right)^2\right) + \frac{4H}{f_0}\left(\mathbf{1}^\top \boldsymbol{b}\right)^2 \widehat{\delta}_2\Big] K\\ + \frac{1}{4}\left(\overline{L}^2 + \left(\mathbf{1}^\top \boldsymbol{b}\right)^2\right)^2 - \overline{L}^2\left(\mathbf{1}^\top \boldsymbol{b}\right)^2 = 0.\end{aligned} \tag{24}$$

To establish the EFCPR of the aggregator, $\mathcal{K}(\cdot)$, the constraint (1) is rewritten as (25) by replacing $\boldsymbol{\beta}^\top \boldsymbol{v}$ with $\mathcal{K}(\cdot)V_{\mathrm{agg}}$.

$$\mathbf{1}^\top \boldsymbol{R} + \widehat{\alpha}(\cdot)\mathbf{1}^\top \boldsymbol{b} + \mathcal{K}(\cdot)V_{\mathrm{agg}} \geq \nu(\cdot) \tag{25}$$

$$\underbrace{4\left(\frac{2H}{f_0}\varpi-\frac{1}{2}\boldsymbol{T}^\top\boldsymbol{v}\right)^2}_{a}K^4+\underbrace{\left\{4\left(\frac{2H}{f_0}\varpi-\frac{1}{2}\boldsymbol{T}^\top\boldsymbol{v}\right)\left[2\left(\frac{2H}{f_0}\varpi-\frac{1}{2}\boldsymbol{T}^\top\boldsymbol{v}\right)K_{\mathrm{V}}-\widehat{L}\right]+\frac{16H}{f_0}\left(\mathbf{1}^\top\boldsymbol{b}\right)^2\widetilde{\delta}_2\right\}}_{b}K^3$$
$$+\underbrace{\left\{\left[2\left(\frac{2H}{f_0}\varpi-\frac{1}{2}\boldsymbol{T}^\top\boldsymbol{v}\right)K_{\mathrm{V}}-\widehat{L}\right]^2-4\left(\frac{2H}{f_0}\varpi-\frac{1}{2}\boldsymbol{T}^\top\boldsymbol{v}\right)\left[\widehat{L}-2\left(\mathbf{1}^\top\boldsymbol{b}\right)\widetilde{L}\right]K_{\mathrm{V}}-4\left(\mathbf{1}^\top\boldsymbol{b}\right)^2\widetilde{L}^2+\frac{16H}{f_0}\left(\mathbf{1}^\top\boldsymbol{b}\right)^2\widetilde{\delta}_2K_{\mathrm{V}}\right\}}_{c}K^2$$
$$\underbrace{-2\left\{\left[2\left(\frac{2H}{f_0}\varpi-\frac{1}{2}\boldsymbol{T}^\top\boldsymbol{v}\right)K_{\mathrm{V}}-\widehat{L}\right]\left[\widehat{L}-2\left(\mathbf{1}^\top\boldsymbol{b}\right)\widetilde{L}\right]K_{\mathrm{V}}\right\}}_{d}K+\underbrace{\left[\widehat{L}-2\left(\mathbf{1}^\top\boldsymbol{b}\right)\widetilde{L}\right]^2K_{\mathrm{V}}^2}_{e}=0 \tag{19}$$

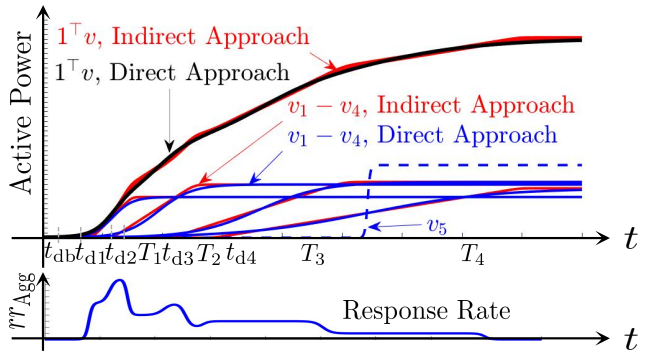

Fig. 3. Illustration of the active power response of aggregated resources.

where $V_{\mathrm{agg}}=\mathbf{1}^\top\boldsymbol{v}$, $\widehat{\alpha}(\cdot)$ and $\mathcal{K}(\cdot)$ are, respectively, given by

$$\widehat{\alpha}(\cdot)=\max\left\{1,\frac{\left(t_{\mathrm{nad}}-t_{\mathrm{db}}-t_{\mathrm{d}}\right)\widehat{K}_{\min}}{L-V_{\mathrm{agg}}-\mathbf{1}^\top\boldsymbol{b}}\right\} \tag{26}$$
$$\mathcal{K}(\cdot)=\max\left\{1,\widehat{\varphi}(T_{\mathrm{agg}},K_{\mathrm{agg}})\widehat{\alpha}(\cdot)\right\} \tag{27}$$

where $\widehat{\varphi}(T_{\mathrm{agg}},K_{\mathrm{agg}})$ and S_{agg} are the terms to be determined.

Similar to the previous subsection, we still believe that the differences of the EFCPR of two aggregators (an aggregator and a provider of $\boldsymbol{b}$) are primarily driven by two factors, i.e., the overall ramping rates of aggregators and the overall delivery time. This can be further clarified using Fig. 4. On the one hand, it is the higher overall ramping rate of aggregators that results in larger EFCPR values primarily driven by the ramping rates of the internal resources. This can be achieved by moving the point in the vertical and horizontal directions as shown in Fig. 4. On the other hand, when the aggregators have the same overall ramping rates, it is the time delays that mainly contribute to the differences. Please see the thin red solid line and thin blue solid line as shown in Fig. 4, their corresponding resources have the same ramping rates, but the their time delays are distinct ($t_{\mathrm{d}1}\rightarrow t'_{\mathrm{d}1}$, $t'_{\mathrm{d}2}\rightarrow t''_{\mathrm{d}2}$). Generally, we have a common view that resources with lower latency will have better performance. Therefore, resources with faster ramping rates and lower time delays are more attractive.

With this in mind, $\widehat{\varphi}(K_{\mathrm{agg}},t_{\mathrm{d,agg}})$ is conservatively modeled as the following form

$$\widehat{\varphi}(K_{\mathrm{agg}},t_{\mathrm{d,agg}})=\frac{K_{\mathrm{agg}}}{e^{\mu*t_{\mathrm{d,agg}}}}=\frac{\mathbf{1}^\top\boldsymbol{v}}{T_{\mathrm{agg}}*e^{\mu*t_{\mathrm{d,agg}}}} \tag{28}$$

where $T_{\mathrm{agg}}=\max\{T_i+t_{\mathrm{d}i}\}-\min\{t_{\mathrm{d}i}\}$, $t_{\mathrm{d,agg}}=\min\{t_{\mathrm{d}i}\}$, $i\in\mathcal{A}^j_{\mathrm{agg}}$, and μ can be properly selected. If multiple aggregators are considered, then, the term $\mathcal{K}(\cdot)V_{\mathrm{agg}}$ will be replaced with $\mathbf{K}(\cdot)^\top\boldsymbol{V}_{\mathrm{agg}}$, where $\mathbf{K}(\cdot)^\top=\left[\mathcal{K}(\cdot)_1,\cdots,\mathcal{K}(\cdot)_{|\mathcal{A}_{\mathrm{agg}}|}\right]$, and $\boldsymbol{V}_{\mathrm{agg}}=\left[V_{\mathrm{agg},1},\cdots,V_{\mathrm{agg},|\mathcal{A}_{\mathrm{agg}}|}\right]^\top$. And in Eq. (23), the term $T_{\mathrm{agg}}V_{\mathrm{agg}}-S_{\mathrm{agg}}$ and $L-V_{\mathrm{agg}}$ will be replaced with $\boldsymbol{T}^\top_{\mathrm{agg}}\boldsymbol{V}_{\mathrm{agg}}-\mathbf{1}^\top\boldsymbol{S}_{\mathrm{agg}}$ and $L-\mathbf{1}^\top\boldsymbol{V}_{\mathrm{agg}}$, respectively, where $\boldsymbol{T}^\top_{\mathrm{agg}}=\left[T_{\mathrm{agg},1},\cdots,T_{\mathrm{agg},|\mathcal{A}_{\mathrm{agg}}|}\right]$ and $\boldsymbol{S}^\top_{\mathrm{agg}}=\left[S_{\mathrm{agg},1},\cdots,S_{\mathrm{agg},|\mathcal{A}_{\mathrm{agg}}|}\right]$. Thus, the performance of resources can be distinguished.

To calculate $S_{\mathrm{agg},j}$, two approaches are proposed as follows.

1) Indirect Approach: In this approach, the aggregated response dynamics $v^j_{\mathrm{agg}}(t)$ is derived through modeling the ramp rate of the aggregated resources $rr^j_{\mathrm{agg}}(t)$. A *Sigmoid*-function-based model (29) is proposed to approximately describe this aggregated ramp rate with the assumption that the ramp rate of these resources is constant during the response period. This can be realized by summarizing the ramp rate of each resource. Please refer to the example shown in Fig. 3 where the blue solid line represents the aggregated ramp rate $rr^j_{\mathrm{agg}}(t)$.

$$rr^j_{\mathrm{agg}}(t)=\sum_{i=1}^{|\mathcal{A}^j_{\mathrm{agg}}|}\left(\frac{k_i}{1+e^{-\sigma_i(t-\rho_i t_{\mathrm{d}i})}}-\frac{k_i}{1+e^{-\sigma_i(t-\gamma_i T_i)}}\right) \tag{29}$$

where k_i is the ramp rate of resource i during the period $[t_{\mathrm{db}}+t_{\mathrm{d}i},t_{\mathrm{db}}+t_{\mathrm{d}i}+T_i]$, $|\mathcal{A}^j_{\mathrm{agg}}|$ is the number of the resources within aggregator j, σ_i, ρ_i and γ_i are constants. Then, the aggregated frequency response dynamics, $v^j_{\mathrm{agg}}(t)$, can be calculated by integrating the ramp rate:

$$v^j_{\mathrm{agg}}(t)=\sum\nolimits_{i=1}^{|\mathcal{A}^j_{\mathrm{agg}}|}\left(\frac{k_i}{\sigma_i}\ln\frac{1+e^{\sigma_i(t-\rho_i t_{\mathrm{d}i})}}{1+e^{\sigma_i(t-\gamma_i T_i)}}\right)+C^j_{\mathrm{agg}} \tag{30}$$

where T_i is the response time of resource i, C^j_{agg} is a constant and is given by $C^j_{\mathrm{agg}}=\sum_{i=1}^{|\mathcal{A}^j_{\mathrm{agg}}|}\left(\frac{k_i}{\sigma_i}\ln\frac{1+e^{-\sigma_i\gamma_i T_i}}{1+e^{-\sigma_i\rho_i t_{\mathrm{d}i}}}\right)$. Then, we can calculate $S_{\mathrm{agg},j}$ as follows.

$$\begin{aligned}S_{\mathrm{agg},j}&=\int_0^{T_{\mathrm{agg},j}+t_{\mathrm{db}}+t^j_{\mathrm{d,agg}}}v^j_{\mathrm{agg}}(t)\,dt\\&=\sum_{i=1}^{|\mathcal{A}^j_{\mathrm{agg}}|}\frac{k_i}{\sigma_i^2}\Big[\widehat{\chi}_i(\ln\widehat{\chi}_i-1)-\widehat{\hbar}_i\Big(\ln\widehat{\hbar}_i-1\Big)-\chi_i(\ln\chi_i-1)\\&\quad+\hbar_i(\ln\hbar_i-1)\Big]+C^j_{\mathrm{agg}}\left(T_{\mathrm{agg},j}+t_{\mathrm{db}}+t^j_{\mathrm{d,agg}}\right)\end{aligned} \tag{31}$$

where $\chi_i=1+e^{\sigma_i\rho_i t_{\mathrm{d}i}}$, $\widehat{\chi}_i=1+e^{-\sigma_i\left(T_{\mathrm{agg},j}+t_{\mathrm{db}}+t^j_{\mathrm{d,agg}}-\rho_i t_{\mathrm{d}i}\right)}$, $\hbar_i=1+e^{\sigma_i\gamma_i T_i}$, $\widehat{\hbar}_i=1+e^{-\sigma_i\left(T_{\mathrm{agg},j}+t_{\mathrm{db}}+t^j_{\mathrm{d,agg}}-\gamma_i T_i\right)}$.

Once the parameter $S_{\mathrm{agg},j}$ is obtained, the overall EFCPR of the aggregated resources, $\mathcal{K}(\cdot)_j$, can be calculated through (23), (26), and (27).

$$\widehat{K}_{\min}=\frac{\left\{\mathbf{1}^\top\boldsymbol{b}\sqrt{\Delta_3}-\sqrt{\left[\Delta_2+\Delta_3-\frac{f_0}{2H}\left(Lt_d+T_{\text{agg}}V_{\text{agg}}-S_{\text{agg}}\right)\right](L-V_{\text{agg}})^2-\left[\Delta_2-\frac{f_0}{2H}\left(Lt_d+T_{\text{agg}}V_{\text{agg}}-S_{\text{agg}}\right)\right](\mathbf{1}^\top\boldsymbol{b})^2}\right\}^2}{\frac{4H}{f_0}\left[\Delta_2+\Delta_3-\frac{f_0}{2H}\left(Lt_d+T_{\text{agg}}V_{\text{agg}}-S_{\text{agg}}\right)\right]^2} \tag{23}$$

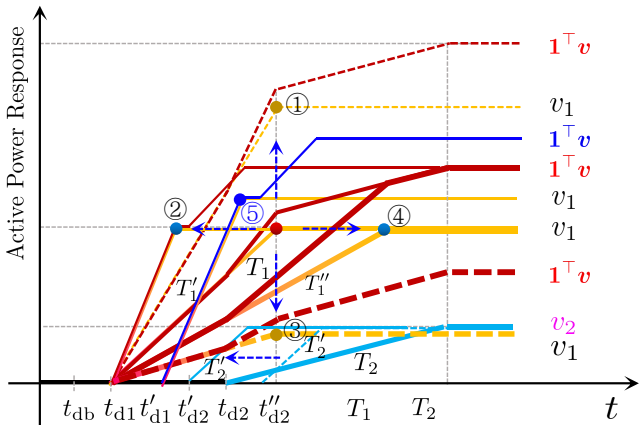

Fig. 4. Illustration of Impacts of Ramping Rates and Time Delay.

2) Direct Approach: In this approach, the aggregated response dynamics, $v_{\text{agg}}^j(t)$, is directly and approximately derived based on the *Sigmoid* function, i.e.,

$$v_{\text{agg}}^j(t)=\sum\nolimits_{i=1}^{|\mathcal{A}_{\text{agg}}^j|}\frac{v_i}{1+e^{-\overline{\sigma}_i[t-\overline{\rho}_i(T_i+t_{\text{d}i}+t_{\text{db}})]}} \tag{32}$$

where $\overline{\sigma}_i$ and $\overline{\rho}_i$ are constants. Then, with similar methods to (31), we can get the parameter $S_{\text{agg},j}$:

$$S_{\text{agg},j}=\sum_{i=1}^{|\mathcal{A}_{\text{agg}}^j|}\frac{v_i}{\overline{\sigma}_i}\left[\ln\frac{1+e^{\overline{\sigma}_i\left[T_{\text{agg},j}+t_{\text{d,agg}}^j+t_{\text{db}}-\overline{\rho}_i(T_i+t_{\text{d}i}+t_{\text{db}})\right]}}{1+e^{-\overline{\sigma}_i\overline{\rho}_i(T_i+t_{\text{d}i}+t_{\text{db}})}}\right] \tag{33}$$

where v_i can be replaced with k_iT_i.

In fact, K_{agg} in (28) can be replaced with rr_{agg}^j in (29), then $\widehat{\varphi}(K_{\text{agg}},t_{\text{d,agg}})$ is essentially a time-varying parameter. Of cause, $S_{\text{agg},j}$ can be approximately calculated by using (34) if there is no need to avoid the piece-wise linear characteristics.

$$S_{\text{agg},j}=\frac{1}{2}\sum\nolimits_{i=1}^{|\mathcal{A}_{\text{agg}}^j|}v_iT_i=\frac{1}{2}\boldsymbol{T}^{j\top}\boldsymbol{v}^j \tag{34}$$

where $\boldsymbol{T}^{j\top}$ and $\boldsymbol{v}^j$ are the delivery time vector and response volume of resources in aggregator j, respectively.

***Remark* 2.** *Both indirect and direct approaches can be used appropriately to approximately calculate S_{agg}, but it could be more complex by using the former approach. Other approaches to calculate S_{agg} could be explored as well such as the method proposed in [34] based on Padé-approximation. Additionally, if $\boldsymbol{b}$ is deployed before that from the aggregated resources is fully delivered, i.e., $t_2<T_{agg}$, it could be difficult to directly calculate the ratios $\widehat{\alpha}(\cdot)$ and $\mathcal{K}(\cdot)$ through the proposed direct and indirect approaches when deriving the parameters t_2 and K_{min} due to the composite function composed of exponential and logarithmic functions. However, the parameter t_2 could still be approximately obtained, and then the ratios $\widehat{\alpha}(\cdot)$ and $\mathcal{K}(\cdot)$, which will be discussed in the following subsection. Regarding the parameters of the sigmoid function, such as k_i, T_i, t_{di}, σ_i, ρ_i and γ_i in (29), the resources within the aggregator usually undergo qualification test before officially providing corresponding response services to the power grid, and only those who have passed the test can provide services through the aggregator. Aggregators can use the collected data during these tests to determine the parameters of the sigmoid function and make corrections in practical applications.*

E. EFCPR of Aggregated Resources When $t_2<T_{agg}$

In this subsection, we try to derive the ratios $\widehat{\alpha}(\cdot)$ and $\mathcal{K}(\cdot)_j$ by extending the results in above subsection to the scenario that $\boldsymbol{b}$ is delivered before the time when the support from the aggregated resources is fully delivered, i.e., $t_2<T_{\text{agg},j}$. Taking similar steps, we have

$$Kt_2^2+2S_{\text{agg},j}^{\overleftarrow{t_2}}+\frac{4H}{f_0}\delta_2-2LT_{\text{agg},j}=0 \tag{35}$$

where $S_{\text{agg},j}^{\overleftarrow{t_2}}$ is the energy provided by the aggregated resources by the time t_2, and can be calculated with the direct approach (33) by replacing $T_{\text{agg},j}$ with t_2.

Let $S_{\text{agg},j}^0=\sum_{i=1}^{|\mathcal{A}_{\text{agg}}^j|}\frac{v_i}{\overline{\sigma}_i}\ln\left[1+e^{-\overline{\sigma}_i\overline{\rho}_i(T_i+t_{\text{d}i}+t_{\text{db}})}\right]$, then (35) can be rewritten as

$$2\sum_{i=1}^{|\mathcal{A}_{\text{agg}}^j|}\frac{v_i}{\overline{\sigma}_i}\ln\left[1+e^{\overline{\sigma}_i\left[t_2+t_{\text{d,agg}}^j+t_{\text{db}}-\overline{\rho}_i(T_i+t_{\text{d}i}+t_{\text{db}})\right]}\right]+Kt_2^2+\frac{4H}{f_0}\delta_2-2LT_{\text{agg},j}-2S_{\text{agg},j}^0=0. \tag{36}$$

To derive t_2, we use Taylor series expansion and take the first three terms to approximate the logarithmic function in (36). Then, (36) can be further written as

$$\left(K+\sum_{i=1}^{|\mathcal{A}_{\text{agg}}^j|}\frac{v_i}{\overline{\sigma}_i}\eta_i''(t_2^\circ)\right)t_2^2+2\sum_{i=1}^{|\mathcal{A}_{\text{agg}}^j|}\frac{v_i}{\overline{\sigma}_i}\left(\eta_i'(t_2^\circ)-\eta_i''(t_2^\circ)t_2^\circ\right)t_2+2\sum\nolimits_{i=1}^{|\mathcal{A}_{\text{agg}}^j|}\frac{v_i}{\overline{\sigma}_i}\left(\frac{1}{2}\eta_i''(t_2^\circ)t_2^{\circ2}-\eta_i'(t_2^\circ)t_2^\circ+\eta_i(t_2^\circ)\right)+\frac{4H}{f_0}\delta_2-2LT_{\text{agg},j}-2S_{\text{agg},j}^0=0. \tag{37}$$

where t_2° represents the operating point of the BESS, and $\eta_i(t_2^\circ)$, $\eta_i'(t_2^\circ)$ and $\eta_i''(t_2^\circ)$ are the values of the logarithmic function and its first and second derivatives at t_2°. By solving this equation, we have t_2:

$$t_2=\frac{1}{K+K_{\text{agg}}^{t_2^\circ,j}}\left(L_{\text{agg}}^{\circ,j}-\sqrt{L_{\text{agg}}^{\circ,j2}-\frac{4H}{f_0}\left(K+K_{\text{agg}}^{t_2^\circ,j}\right)\delta_{2,\text{agg}}^j}\right) \tag{38}$$

where $K_{\text{agg}}^{t_2^\circ,j}=\sum_{i=1}^{|\mathcal{A}_{\text{agg}}^j|}\frac{k_iT_i}{\overline{\sigma}_i}\eta_i''(t_2^\circ)$,
$\delta_{2,\text{agg}}^j=\delta_2-\frac{f_0}{2H}\left(LT_{\text{agg},j}+S_{\text{agg},j}^0-\eta_{\text{agg}}^{\circ,j}\right)$,
$L_{\text{agg}}^{\circ,j}=\sum_{i=1}^{|\mathcal{A}_{\text{agg}}^j|}\frac{k_iT_i}{\overline{\sigma}_i}\left(\eta_i''(t_2^\circ)t_2^\circ-\eta_i'(t_2^\circ)\right)$, and
$\eta_{\text{agg}}^{\circ,j}=\sum_{i=1}^{|\mathcal{A}_{\text{agg}}^j|}\frac{k_iT_i}{\overline{\sigma}_i}\left(\frac{1}{2}\eta_i''(t_2^\circ)t_2^{\circ2}-\eta_i'(t_2^\circ)t_2^\circ+\eta_i(t_2^\circ)\right)$.

TABLE I
DATA SUMMARIZED ACCORDING TO THE REQUIREMENT OF ERCOT

Parameters	Values	Parameters	Values
f_0 (Hz)	60	f_{db} (Hz)	59.9833
f_{nad} (Hz)	59.4	f_2 (Hz)	59.8
L (MW)	2750	t_{d} (s)	0.2
$\Delta_1 = f_0 - f_{\text{db}}$ (Hz)	0.0167	$\Delta_2 = f_{\text{db}} - f_2$ (Hz)	0.1833
$\Delta_3 = f_0 - f_{\text{nad}} - \Delta_1 - \Delta_2$ (Hz)	0.4	H (GWs), $v(\cdot)$ (MW), $\alpha(\cdot)$	Refer to [36]

The equation (38) has the same form as (18), a four-order equation still should be solved to obtain the minimum K. This can be realized with the help of computer. Additionally, we can use (34) along with the method in previous subsection to do this for simplicity but will not discuss it further.

III. NUMERICAL STUDIES

This section aims to analyze the impacts of parameters on the proposed model and validate the effectiveness of the model. In the numerical studies, the data is set according to the requirements of ERCOT NPRR 863 [35], and parameters appearing in [36] are adopted. These are shown in Table I.

A. Impacts of Parameters on $T_{max}(\cdot)$

We start from analyzing the impacts of different parameters on the time function $T_{\max}(\cdot)$. Fig. 5(a) shows the curve of $T_{\max}(\cdot)$ versus the total system inertia H for different battery reserves $\overline{b} = \mathbf{1}^\top \boldsymbol{b}$ and RES reserves $\overline{v} = \mathbf{1}^\top \boldsymbol{v}$. It can be observed that this function $T_{\max}(\cdot)$ is increasing with the total system inertia and could be appropriately approximated as a linear function of the total system inertia when the variables $\mathbf{1}^\top \boldsymbol{b}$ and $\mathbf{1}^\top \boldsymbol{v}$ are fixed. This result is in line with our operation experience that the higher system inertia the more time the system needs to reach nadir frequency. When the total system inertia H is fixed, the value of the function $T_{\max}(\cdot)$ is also increasing in $\mathbf{1}^\top \boldsymbol{b}$ and $\mathbf{1}^\top \boldsymbol{v}$, which can also be observed from Fig. 5(b), where it shows the curve of $T_{\max}(\cdot)$ versus $\mathbf{1}^\top \boldsymbol{b}$ for different system inertia levels when $\mathbf{1}^\top \boldsymbol{v} = 0$, and Fig. 5(d) where it shows the curve of $T_{\max}(\cdot)$ versus $\mathbf{1}^\top \boldsymbol{v}$ for different system inertia levels and battery reserves for fast frequency control. Fig. 5(b) and Fig. 5(d) also demonstrate the significant impacts of $\mathbf{1}^\top \boldsymbol{b}$ and $\mathbf{1}^\top \boldsymbol{v}$ on the $T_{\max}(\cdot)$. However, as seen in Fig. 5(d), $T_{\max}(\cdot)$ varies slightly in the total RES reserve $\mathbf{1}^\top \boldsymbol{v}$ at high inertia level and low battery reserve level at which the function can be properly approximated as being constant in the total RES reserve $\mathbf{1}^\top \boldsymbol{v}$, and which is mainly caused by the time $\boldsymbol{T}$. This parameter could weaken the influence of RES reserve $\mathbf{1}^\top \boldsymbol{v}$ on $T_{\max}(\cdot)$. Additionally, a common feature that can be extracted from the above results is that more primary frequency control reserves provided by batteries and RES will make the time $T_{\max}(\cdot)$ longer. The main reason is that it's equivalent to increase the overall ramp rate of the system and reduce the power loss, slowing down the decline of the frequency. Therefore, it will take more time to reach the same nadir frequency.

Following, the impacts of the response time $\boldsymbol{T}$, time delay t_d and the triggering time instant Δ_2 on $T_{\max}(\cdot)$ are also discussed. The results are shown in Fig. 5(c), (e) and (f). Fig. 5(c) shows the value of the function $T_{\max}(\cdot)$ versus the response time $\boldsymbol{T}$ for different total system inertia. It is shown that the value of $T_{\max}(\cdot)$ decreases as long as the response time increases, and this relationship can be appropriately approximated as being a decreasing linear function of the response time. When the other parameters are fixed, increasing $\boldsymbol{T}$ means equivalently reducing the overall system ramp according to Fig. 1, speeding up the drop in frequency and consequently reducing the time it takes to reach the same frequency nadir.

B. Validation of EPFRCR Model

1) ERCOT System Case: In the following, the proposed EPFRCR model is validated using the empirical results of the ERCOT system from [36] and compared with the existing work [40], [41]. Fig. 6(a) shows the values of $\frac{(t_{\text{nad}} - t_{\text{db}} - t_{\text{d}}) K_{\min}}{L - \mathbf{1}^\top \boldsymbol{v} - \mathbf{1}^\top \boldsymbol{b}}$ versus the total system inertia, where the dash-dotted orange line is obtained using the empirical results from [36], the dashed blue line is obtained by using the model proposed in [40], and the solid-red line is obtained by using our proposed model in this paper. It is observed that the proposed model can appropriately approximate the ratio, and better than the existing work, particularly at lower inertia levels. The root mean square error (RMSE) is further used to quantify the accuracy of the proposed model. The results from [36] are regarded as true values, then the RMSE values using the model from [40] and our proposed model are 0.263 and 0.119, respectively, showing the superiority of the proposed model.

Fig. 6(a) also shows the variation trend of both $\alpha(\cdot)$ for $\boldsymbol{b}$ and $\beta(\cdot)$ for $\boldsymbol{v}$ with total system inertia H for different response times when $\mathbf{1}^\top \boldsymbol{v} = \mathbf{1}^\top \boldsymbol{b} = 200$ MW. It can be found that 1) the value of the EFCPR decreases with the increase of total system inertia, which means that the fast-acting batteries and RES perform much better at lower inertia levels in primary frequency control, and these resources have almost the same performance when the total system inertia is large enough; 2) generally, resources with less response time have higher EFCPR values (perform much better or more effective).

2) GB System Case: To further demonstrate the effectiveness of the proposed model, the GB power system data including system inertia, DCL, DML, SFFR, and mandatory frequency response (primary) from September 30, 2023 to December 2, 2024 are used to calculate the EFCPR values. These data are collected and reorganized through ModoEnergy [48] and NESO websites [49]–[52]. The technical requirements for these response services can be found on the NESO website and in the files [46], [53]. Here we mainly focus on calculating the EFCPR of DCL, and the result is presented in Fig. 6(c), showing the trend of EFCPR of DCL variation with total system inertia. The DCL EFCPR values are distributed mainly in the range of 1.5 to 4 when the system inertia is higher than 80 GWs and lower than 150 GWs. This result is well line with the so-called exchange rate published by NESO recently (DCL–1.5 to 4.3) [54], demonstrating the effectiveness of the proposed model. Furthermore, noting the trend of reduction of system inertia shown in Fig. 6(b), the DCL EFCPR values could be increased in the future.

3) EFCPR Values of Aggregated Resources: Finally, we try to calculate the EFCPR values of various aggregated resources still by using GB system data collected from NESO websites [49]–[52] which allows us to observe the distribution of resources providing different frequency response services (SFFR and DCL) (schematically shown in Fig. 7). With this information, four categories of aggregated resources are considered, i.e., Agg1, Agg2, Agg3, and Agg4. These aggregators

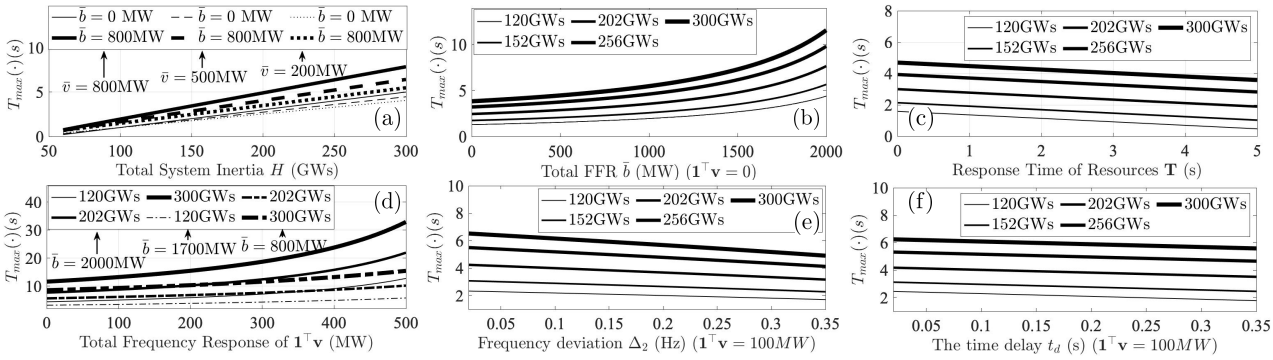

Fig. 5. Impacts of parameters on values of the function $T_{\max}(\cdot)$.

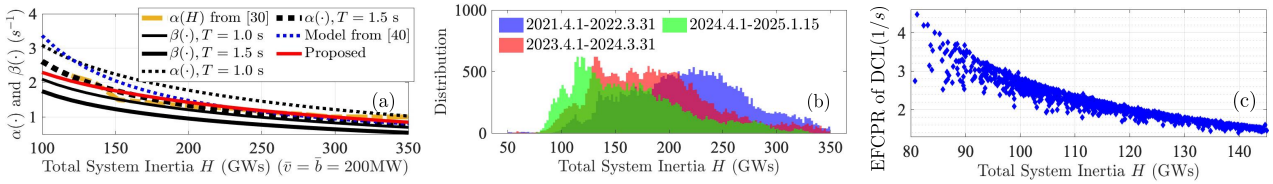

Fig. 6. The results of calculated EFCPR values using modified ERCOT test case and GB power grid with real operational data.

TABLE II
MAIN DETAILS ABOUT THE AGGREGATED RESOURCES ($Agg1-Agg4$)

Aggregators	Resources	Services	Parameters
Agg1	BESS+Load Response	DCL+SFFR	$T_{agg1}=3s$
Agg2	BESS+Load Response	DCL+SFFR	$T_{agg2}=2s$
Agg3	BESS+Diesel	DCL+SFFR	$T_{agg3}=5s$
Agg4	BESS (DCL)+Diesel+Battery (SFFR)	DCL+SFFR	$T_{agg4}=4s$

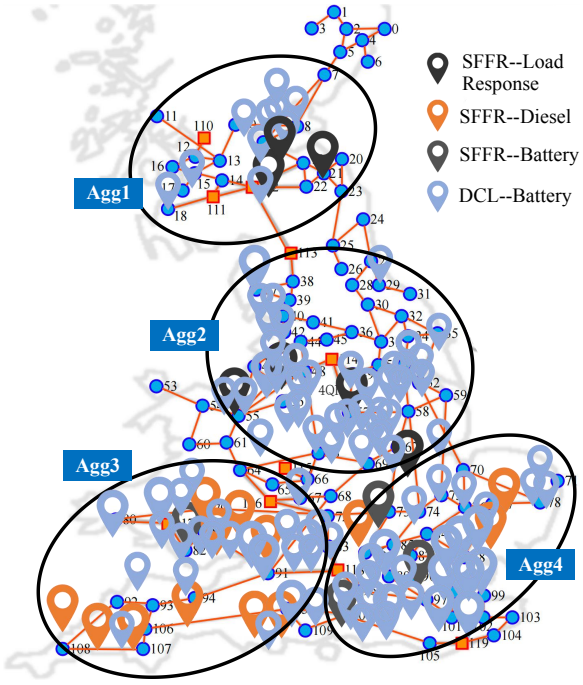

Fig. 7. Illustration of the Distribution of Resources Providing DCL and SFFR Services Using GB Power Grid as an Example.

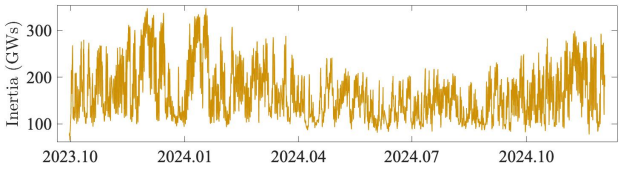

Fig. 8. Total System Inertia of GB Power Grid from Sep. 30, 2023 to Dec. 02, 2024, which is collected from [49].

simultaneously provide DCL and SFFR services. The details are presented in Table II. Besides, the total system inertia in GWs from September 30, 2023 to December 02, 2024 is also presented in Fig. 8. Here, only the direct approach (32) and (33) is used to calculate the parameter S_{agg} and then the EFCPR values. The results are shown in Fig. 9, clearly showing the EFCPR values of the aggregators and that of the DCL service. Behind the differences of the EFCPR values of the aggregators lies primarily two folds as discussed in previous sections, i.e., the overall ramping rates and the time delay. The percent of DCL in the aggregators (the top subfigure in Fig. 9) means different ramping rates. The higher proportion of DCL volumes in the aggregators the larger EFCPR values are when the aggregators have the same time delay. Furthermore, it can be observed that the EFCPR values vary more dramatically (more sensitively) when the system is at lower levels of inertia (compared with Fig. 8). This is totally in line with the results shown in Fig. 6(b), and may bring great opportunities for fast-acting resources.

IV. DISCUSSION

The proposed model leads to complex and highly nonlinear relationships between reserve provisions and the ratio. The frequency control reserve directly affects the relative effectiveness of resources in controlling frequency. Conversely, the proposed model, i.e., EFCPR, will affects the decision of the frequency control reserves seen from (1). Furthermore, the

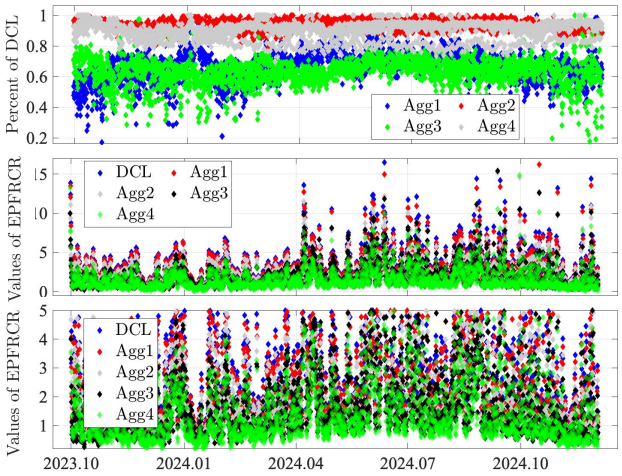

Fig. 9. Results of EFCPR. (Top sub figure: Percent of DCL in four aggregators; Middle sub figure: EFCPR values of aggregators; Bottom sub figure: Zoom in of the middle sub figure.)

EFCPR is an uncertain variable due to the stochastic nature of the system inertia H. Therefore, if the EFCPR, i.e., $\alpha(\cdot)$ and $\boldsymbol{\beta}(\cdot)$, are utilized by system operators to procure the frequency control reserves, this problem could be formulated as a so-called decision-dependent stochastic optimization problem. This could be a challenging but meaningful issue, particularly if the relationships between reserve provisions and the ratio are complex and highly nonlinear. In fact, some researchers have explored and published several excellent works recent years. Although this topic is beyond the scope of this paper, it could be valuable to explore a closed-loop solution of "Prediction-Decision-Prediction" to solve this optimization problem, making the proposed model more practical.

The second issue could be that full data access and linear responses are assumed to compute the ratio in this paper. It is practical to assume linear response as existing works did. The data of system inertia H, power loss L, and frequency control reserves such as $\boldsymbol{b}$ and $\boldsymbol{v}$ are required to compute the ratio. The massive historical operational data about these parameters could be fully utilized to forecast the EFCPR values, revealing the changing patterns of EFCPR. And the frequency control reserve decisions may be then utilized to adjust the values of EFCPR. Advanced algorithms such as deep learning based methods can also be developed to address the issue of data scarcity. The above mentioned closed-loop solution combining with deep learning based advanced methods [55], [56] could be helpful to address the uncertainty and assumptions of full data access and linear responses issues.

Moreover, detailed data about all resources such as response times and ramp rates will be required as well to calculate the ratios. However, If only partial or estimated data is available in practice, the system operator, could configure appropriate parameters for resources lacking available data based on resource types, qualification test data, and operating experience in order to calculate EFCPR. On the other hand, the system operator may utilize some other data such as resource historical or real-time output power data to identify these required parameters.

Additionally, parameters of all SGs are set to be the same such as T_g, and it is assumed that all SGs deliver the PFR reserve with constant aggregate ramp rate K. In fact, this is a conservative model since some SGs may deploy all PFR reserve before the frequency nadir is reached. If we would like to consider the heterogeneous SG governor designs in the model, SGs with very similar parameters can be aggregated into one and SGs with faster ramping rates can be modeled as similar to the resources that provide $\boldsymbol{v}$. By doing so and rearranging (1) and (2), the proposed method can be used to evaluate the service performance of heterogeneous SGs.

V. Conclusions

This paper provides an analytical model, EFCPR, for heterogeneous resources to accurately quantify their relative effectiveness to conventional SGs in providing frequency response services, where various response characteristics of resources are taken into account. The extension of the EFCPR model to aggregated resources and a more general scenario considering the delivery time instant of BESS that can immediately release the expected energy is further investigated based on Sigmoid function. The proposed EFCPR model has been numerically validated by using both the Texas test case and the GB power grids with the latest real data collected from the NESO website for over a year. The results perfectly match both the empirical operation data from ERCOT and the exchange rate published by NESO recently, demonstrating the effectiveness of this model and penetrating many of parameters' impacts.

However, the work in this field is still in its infancy, requiring more extensive and in-depth studies. Various parameters affect the EFCPR values, some of which are uncertain and variable such as system inertia or difficult to be accurately known like the size of power loss. Therefore, it could be valuable to discuss the probabilistic forecast of EFCPR values in future work. A second one is the EFCPR values of services at different locations. Behind the EFCPR model lies a hidden assumption that all generators, loads and converter-based resources are assumed to be connected to the same bus, ignoring the impacts of grid topology. Actually, the resources interact with each other via power grids, and the inertia level and characteristics of resources vary with different regions, inevitably resulting in distinct distribution of EFCPR values. Additionally, day-ahead scheduling and real-time dispatch, which take the EFCPR of services into account, are also necessary, which is what we are currently carrying out. Particularly, this problem could be formulated as a challenging but meaningful decision-dependent stochastic optimization, where the EFCPR is closely related to the decision variables. The proposed method can be extended to evaluate the inertia response performance as well, which needs further exploration.

Appendix

A. Derivation of Equation (6)

Combining Fig. 1, Eqs. (2)-(5), and the definition of Δ_1 and δ_1, we can have

$$2H\Delta_1/f_0 = Lt_{db} \Rightarrow t_{\mathrm{db}} = 2H\Delta_1/Lf_0 \tag{A1}$$

With this result and take similar operations, we have

$$2H(\Delta_1+\delta_1)/f_0 = L(t_{db}+t_d) \Rightarrow \delta_1 = f_0Lt_d/2H \tag{A2}$$

Go a step further, if $f_0 - f(t) = \Delta_1 + \delta_1 + \delta_2$, then we can have (A3) and then (A4). By rearranging equation (A4), equation (A5) can be obtained.

$$\begin{aligned}\frac{2H}{f_0}(\Delta_1+\delta_1+\delta_2) &= A+B+C_1+\cdots+C_{|\mathcal{V}|}+D \\ &= L(t_{db}+t_d)+\frac{1}{2}\left(L+L-v_1-\sum_{i=2}^{|\mathcal{V}|}K_iT_1-KT_1\right)T_1+\frac{1}{2}\left(L-v_1-\sum_{i=2}^{|\mathcal{V}|}K_iT_1-KT_1\right. \\ &\quad \left.+L-v_1-v_2-\sum_{i=3}^{|\mathcal{V}|}K_iT_2-KT_2\right)(T_2-T_1)+\cdots+\frac{1}{2}\left(L-\sum_{i=1}^{|\mathcal{V}|-1}v_i-K_{|\mathcal{V}|}T_{|\mathcal{V}|-1}-KT_{|\mathcal{V}|-1}\right. \\ &\quad \left.+L-\mathbf{1}^\top\boldsymbol{v}-KT_{|\mathcal{V}|}\right)\left(T_{|\mathcal{V}|}-T_{|\mathcal{V}|-1}\right)+\frac{1}{2}\left(L-\mathbf{1}^\top\boldsymbol{v}-KT_{|\mathcal{V}|}+L-\mathbf{1}^\top\boldsymbol{v}-Kt_2\right)\left(t_2-T_{|\mathcal{V}|}\right) \quad \text{(A3)}\end{aligned}$$

$$\begin{aligned}\frac{2H}{f_0}\delta_2 &= \frac{1}{2}\left(2L-v_1-\sum_{i=2}^{|\mathcal{V}|}\frac{v_i}{T_i}T_1-KT_1\right)T_1+\frac{1}{2}\left(2L-2v_1-v_2-\frac{v_2}{T_2}T_1-\sum_{i=3}^{|\mathcal{V}|}\frac{v_i}{T_i}(T_1+T_2)-K(T_1+T_2)\right)(T_2-T_1) \\ &\quad+\frac{1}{2}\left(2L-2(v_1+v_2)-v_3-\frac{v_3}{T_3}T_2-\sum_{i=4}^{|\mathcal{V}|}\frac{v_i}{T_i}(T_2+T_3)-K(T_2+T_3)\right)(T_3-T_2)+\cdots \\ &\quad+\frac{1}{2}\left(2L-2\sum_{i=1}^{|\mathcal{V}|-2}v_i-v_{|\mathcal{V}|-1}-\frac{v_{|\mathcal{V}|-1}}{T_{|\mathcal{V}|-1}}T_{|\mathcal{V}|-2}-\sum_{i=|\mathcal{V}|}^{|\mathcal{V}|}\frac{v_i}{T_i}\left(T_{|\mathcal{V}|-2}+T_{|\mathcal{V}|-1}\right)-K\left(T_{|\mathcal{V}|-2}+T_{|\mathcal{V}|-1}\right)\right)\left(T_{|\mathcal{V}|-1}-T_{|\mathcal{V}|-2}\right) \\ &\quad+\frac{1}{2}\left(2L-2\sum_{i=1}^{|\mathcal{V}|-1}v_i-r_{|\mathcal{V}|}-\frac{v_{|\mathcal{V}|}}{T_{|\mathcal{V}|}}T_{|\mathcal{V}|-1}-K\left(T_{|\mathcal{V}|-1}+T_{|\mathcal{V}|}\right)\right)\left(T_{|\mathcal{V}|}-T_{|\mathcal{V}|-1}\right) \\ &\quad+\frac{1}{2}\left(2L-2\mathbf{1}^\top\boldsymbol{v}-K\left(t_2+T_{|\mathcal{V}|}\right)\right)\left(t_2-T_{|\mathcal{V}|}\right) \quad \text{(A4)}\end{aligned}$$

$$Kt_2^2-2\left(L-\mathbf{1}^\top\boldsymbol{v}\right)t_2+\frac{4H}{f_0}\left(\delta_2-\frac{f_0}{4H}\boldsymbol{T}^\top\boldsymbol{v}\right)=0 \quad \text{(A5)}$$

By solving (A5), we have

$$t_2=\frac{1}{K}\left(\overline{L}-\sqrt{\overline{L}^2-4HK\overline{\delta}_2/f_0}\right) \quad \text{(A6)}$$

where $\overline{L}=L-\mathbf{1}^\top\boldsymbol{v}$, $\overline{\delta}_2=\delta_2-\frac{f_0\boldsymbol{T}^\top\boldsymbol{v}}{4H}$, and the smaller root is picked in (A6) according to Assumption 1. Similarly, if $f_0-f(t)=f_0-f_{\text{nad}}$, then, with a series of mathematical operations, we have

$$\frac{2H}{f_0}\varpi=\frac{\left(L-\mathbf{1}^\top\boldsymbol{v}-\mathbf{1}^\top\boldsymbol{b}\right)^2}{2K}+\frac{1}{2}\boldsymbol{T}^\top\boldsymbol{v}+\left(\mathbf{1}^\top\boldsymbol{b}\right)t_2 \quad \text{(A7)}$$

where $\varpi=f_0-f_{\text{nad}}-\Delta_1-\frac{f_0}{2H}Lt_d$. Combing (A6) and (A7), we can have the following equation.

$$\begin{aligned}&\left(\frac{2H}{f_0}\varpi-\frac{1}{2}\boldsymbol{T}^\top\boldsymbol{v}\right)^2K^2+\left[\left(\frac{1}{2}\boldsymbol{T}^\top\boldsymbol{v}-\frac{2H}{f_0}\varpi\right)\times\right. \\ &\left.\left(\overline{L}^2+\left(\mathbf{1}^\top\boldsymbol{b}\right)^2\right)+\frac{4H}{f_0}\left(\mathbf{1}^\top\boldsymbol{b}\right)^2\overline{\delta}_2\right]K \\ &+\frac{1}{4}\left(\overline{L}^2+\left(\mathbf{1}^\top\boldsymbol{b}\right)^2\right)^2-\overline{L}^2\left(\mathbf{1}^\top\boldsymbol{b}\right)^2=0 \quad \text{(A8)}\end{aligned}$$

By solving equation (A8), equation (6) can be easily obtained.

REFERENCES

[1] Z. Chu, U. Markovic, G. Hug and F. Teng, "Towards optimal system scheduling with synthetic inertia provision from wind turbines," *IEEE Trans. Power Syst.*, vol. 35, no. 5, pp. 4056-4066, Sept. 2020.

[2] J. Matevosyan. ERCOT's Experience Integrating High Shares of IBR [Online]. (6/16/2021) [30/8/2021]. Available: https://www.wingrid.org/wp-content/uploads/2021/08/13-Julia-Matevosyan-ERCOT-Integrating-high-shares-of-IBR.pdf

[3] AEMO. 2020 System Strength and Inertia Report [Online]. (17/12/2020) [18/7/2021] Available: https://www.aemo.com.au/-/media/files/electricity/nem/planning_and_forecasting/Operability/2020/2020-System-Strength-and-Inertia-Report

[4] L. Mehigan, D. A. Kez, S. Collins, A. Foley, B. Ó'Gallachóir, and P. Deane, "Renewables in the European power system and the impact on system rotational inertia," *Energy*, vol. 203, 117776, pp. 1-14, May 2020.

[5] AEMO, Black system south Australia 28 September 2016, 23 March 2017. Available: https://apo.org.au/sites/default/files/resource-files/2017-03/apo-nid74886.pdf.

[6] AEMO. Final Report - Queensland and South Australia system separation on 25 August 2018 [Online]. (10/1/2019) Available: [15/7/2021] https://www.aemo.com.au/-/media/Files/Electricity/NEM/Market_Notices_and_Events/Power_System_Incident_Reports/2018/Qld---SA-Separation-25-August-2018-Incident-Report.pdf

[7] AEMO. Final Report - Victoria and South Australia Separation Event on 31 January 2020 [Online]. (/11/2020) [15/7/2021] Available: https://aemo.com.au/-/media/files/electricity/nem/market_notices_and_events/power_system_incident_reports/2020/final-report-vic-sa-separation-31-jan--2020.pdf?la=en

[8] NGESO, Technical Report on the events of 9 August 2019, 6 September 2019. Available: https://www.nationalgrideso.com/document/152346/download.

[9] ICS Investigation Expert Panel, Continental Europe Synchronous Area Separation on 08 January 2021 Final Report - main report [online]. Available: [10/1/2022] https://eepublicdownloads.azureedge.net/clean-documents/SOC%20documents/SOC%20Reports/entso-e_CESysSep_Final_Report_210715.pdf

[10] M. Paturet, U. Markovic, S. Delikaraoglou, E. Vrettos, P. Aristidou and G. Hug, "Stochastic unit commitment in low-inertia grids," *IEEE Trans. Power Syst.*, vol. 35, no. 5, pp. 3448-3458, Sept. 2020.

[11] Z. Zhang, E. Du, F. Teng, N. Zhang and C. Kang, "Modeling Frequency Dynamics in Unit Commitment With a High Share of Renewable Energy," *IEEE Trans. Power Syst.*, vol. 35, no. 6, pp. 4383-4395, Nov. 2020.

[12] P. Lu, N. Zhang, L. Ye, E. Du and C. Kang, "Advances in model predictive control for large-scale wind power integration in power systems," *Advances in Applied Energy*, vol. 14, 100177, Jul. 2024.

[13] T. Ding, Z. Zeng, M. Qu, J. P. S. Catalão and M. Shahidehpour, "Two-stage chance-constrained stochastic thermal unit commitment for optimal provision of virtual inertia in wind-storage systems," *IEEE Trans. Power Syst.*, vol. 36, no. 4, pp. 3520-3530, July 2021.

[14] L. Yang, Y. Xu, J. Zhou, and H. Sun, "Distributionally Robust Frequency Constrained Scheduling for an Integrated Electricity-Gas System," *IEEE Trans. Smart Grid*, vol. 13, no. 4, pp. 2730-2743, July 2022.

[15] L. Yang, Z. Li, Y. Xu, J. Zhou and H. Sun, "Frequency Constrained Scheduling Under Multiple Uncertainties via Data-Driven Distributionally Robust Chance-Constrained Approach," *IEEE Trans. Susta. Energy*, vol. 14, no. 2, pp. 763-776, April 2023.

[16] T. Baškarad, I. Kuzle and N. Holjevac, "Photovoltaic System Power Reserve Determination Using Parabolic Approximation of Frequency Response," *IEEE Trans. Smart Grid*, 12(4): 3175-3184, July 2021.

[17] Y. Wen, W. Li, G. Huang and X. Liu, "Frequency dynamics constrained unit commitment with battery energy storage," *IEEE Trans. Power Syst.*, vol. 31, no. 6, pp. 5115-5125, Nov. 2016.

[18] T. Xu, W. Jang and T. Overbye, "Commitment of fast-responding storage devices to mimic inertia for the enhancement of primary frequency response," *IEEE Trans. Power Syst.*, 33(2): 1219-1230, March 2018.

[19] H. Golpîra, A. Atarodi, S. Amini, A. R. Messina, B. Francois and H. Bevrani, "Optimal Energy Storage System-Based Virtual Inertia Placement: A Frequency Stability Point of View," *IEEE Trans. Power Syst.*, vol. 35, no. 6, pp. 4824-4835, Nov. 2020.

[20] L. Badesa, F. Teng and G. Strbac, "Simultaneous scheduling of multiple frequency services in stochastic unit commitment," *IEEE Trans. Power Syst.*, vol. 34, no. 5, pp. 3858-3868, Sept. 2019.

[21] V. Trovato, A. Bialecki and A. Dallagi, "Unit commitment with inertia-dependent and multispeed allocation of frequency response services," *IEEE Trans. Power Syst.*, vol. 34, no. 2, pp. 1537-1548, March 2019.

[22] R. Bhana and T. J. Overbye, "The commitment of interruptible load to ensure adequate system primary frequency response," *IEEE Trans. Power Syst.*, vol. 31, no. 3, pp. 2055-2063, May 2016.

[23] Y. Wang, Q. Guo and M. Chen, "Providing load flexiblity by reshaping power profiles of large language models," *Advances in Applied Energy*, vol. 19, 100232, Sep. 2025.

[24] L. Badesa, F. Teng, and G. Strbac, "Optimal portfolio of distinct frequency-response services in low-inertia systems," *IEEE Trans. Power Syst.*, vol. 35, no. 6, pp. 4459-4469, Nov. 2020.

[25] Y. Zhang, H. Cui, J. Liu, F. Qiu, T. Hong, R. Yao, and F. Li, "Encoding Frequency Constraints in Preventive Unit Commitment Using Deep Learning with Region-of-Interest Active Sampling," *IEEE Trans. Power Syst.*, vol. 37, no. 3, pp. 1942-1955, May 2022.

[26] Y. Wen, J. Zhan, C. Y. Chung and W. Li, "Frequency Stability Enhancement of Integrated AC/VSC-MTDC Systems With Massive Infeed of Offshore Wind Generation," *IEEE Trans. Power Syst.*, vol. 33, no. 5, pp. 5135-5146, Sept. 2018.

[27] H. Gu, R. Yan, T. K. Saha, E. Muljadi, J. Tan and Y. Zhang, "Zonal inertia constrained generator dispatch considering load frequency relief," *IEEE Trans. Power Syst.*, vol. 35, no. 4, pp. 3065-3077, July 2020.

[28] S. S. Oskouee, S. Kamali and T. Amraee, "Primary Frequency Support in Unit Commitment Using a Multi-Area Frequency Model With Flywheel Energy Storage," *IEEE Trans. Power Syst.*, 36(6):5105-5119, Nov. 2021.

[29] L. Badesa, F. Teng and G. Strbac, "Conditions for Regional Frequency Stability in Power System Scheduling—Part I: Theory," *IEEE Trans. Power Syst.*, vol. 36, no. 6, pp. 5558-5566, Nov. 2021.

[30] L. Badesa, F. Teng and G. Strbac, "Conditions for Regional Frequency Stability in Power System Scheduling—Part II: Application to Unit Commitment," *IEEE Trans. Power Syst.*, 36(6):5567-5577, Nov. 2021.

[31] V. Trovato, A. Mazza, and G. Chicco, "Flexible operation of low-inertia power systems connected via high voltage direct current interconnectors," *Electric Power Syst. Res.*, vol. 192, 106911, pp. 1-19, March 2021.

[32] A. Tosatto, G. Misyris, A. Junyent-Ferre, F. Teng and S. Chatzivasileiadis, "Towards Optimal Coordination between Regional Groups: HVDC Supplementary Power Control," *IEEE Trans. Power Syst.*, vol. 37, no. 1, pp. 402-415, Jan. 2022.

[33] Y. Wen, C. Y. Chung, Z. Shuai, L. Che, Y. Xiao and X. Liu, "Toward Flexible Risk-Limiting Operation of Multi-Terminal HVDC Grids With Vast Wind Generation," *IEEE Trans. Sustain. Energy*, vol. 11, no. 3, pp. 1750-1760, July 2020.

[34] V. Häberle, L. Huang, X. He, E. Prieto-Araujo, and F. Dörfler, "Dynamic Ancillary Services: From Grid Codes to Transfer Function-Based Converter Control," Available: https://arxiv.org/abs/2310.01552

[35] ERCOT, "NPRR 863: Creation of primary frequency response service product and revisions to responsive reserve," ERCOT, Tech. Rep. NPRR 863, Jan. 2018. [Online]. Available: http://www.ercot.com/mktrules/issues/reports/nprr

[36] C. Liu and P. Du, "Participation of load resources in day-ahead market to provide primary-frequency response reserve," IEEE Trans. Power Syst., vol. 33, no. 5, pp. 5041–5051, Sep. 2018.

[37] W. Li, P. Du, and N. Lu, "Design of a new primary frequency control market for hosting frequency response reserve offers from both generators and loads," IEEE Trans. Smart Grid, 9(5):4883–4892, Sep. 2018.

[38] ERCOT, Item 6: Recommendation regarding 2025 ERCOT Methodologies for Determining Minimum Ancillary Service Requirements, Available: https://www.ercot.com/files/docs/2025/01/27/6-recommendation-regarding-2025-ercot-methodologies-for-determining-minimum-ancillary-service-requirements.pdf

[39] M. Garcia and R. Baldick, "Requirements for Interdependent Reserve Types Providing Primary Frequency Control," IEEE Trans. Power Syst., vol. 37, no. 1, pp. 51-64, Jan. 2022.

[40] M. Garcia and R. Baldick, "Real-time co-optimization: Interdependent reserve types for primary frequency response," in Proc. 10th ACM Int. Conf. Future Energy Syst., 2019, pp. 550–555.

[41] M. Garcia, "Non-convex mypoic electricity markets: The AC transmission network and interdependent reserve types," Ph.D. dissertation, Electrical Computer Engineering University Texas, Austin, 2019.

[42] Y. Yang, J. C. -H. Peng and Z. -S. Ye, "A Market Clearing Mechanism Considering Primary Frequency Response Rate," IEEE Trans. Power Syst., vol. 36, no. 6, pp. 5952-5955, Nov. 2021.

[43] J. Zhou, Y. Guo, Z. Meng, L. Yang and H. Sun, "Regional Frequency Dynamics Modeling of Power Systems Incorporating Frequency Support from HVDC Links and Renewable Energy Sources," 2024 IEEE Power & Energy Society General Meeting (PESGM), Seattle, WA, USA, 2024.

[44] ENTSO-E. Technical Requirements for Fast Frequency Reserve Provision in the Nordic Synchronous Area [Online]. (23/5/2019) [25/8/2021] Available: https://www.epressi.com/media/userfiles/132826/1562134367/technical-requirements-for-fast-frequency-reserve-provision-in-the-nordic-synchronous-area-1.pdf

[45] ERCOT. ERCOT Nodal Protocols [Online]. (December 11, 2024), Available: https://www.ercot.com/files/docs/2024/12/09/December%2011,%202024%20Nodal%20Protocols.pdf

[46] NESO. New Response Services Service Terms [Online], (15/3/2024) [27/2/2025], Available: https://www.neso.energy/document/304441/download

[47] SAMR, and SAC. Code on security and stability of power system (GB 38755-2019) (in Chinese) [Online]. Available: http://c.gb688.cn/bzgk/gb/showGb?type=download&hcno=1D988D54A435E864E67CAA13217E8A99

[48] NESO, https://modoenergy.com/data/plotter/great-britain/live-and-historic-data/balancing-mechanism/bid-offer-volumes?end_date=2024-09-30&fields=%255B%2522VolumeByFuelTypeOther.volume_mwh%2522%255D&start_date=2023-09-30

[49] NESO, https://www.neso.energy/data-portal/system-inertia

[50] NESO, https://www.neso.energy/industry-information/balancing-services/frequency-response-services/static-firm-frequency-response-sffr

[51] NESO, https://www.neso.energy/data-portal/dynamic-containment-data

[52] NESO, https://www.neso.energy/industry-information/balancing-services/frequency-response-services/mandatory-frequency-response-mfr#Technical-requirements

[53] NESO. MANDATORY FREQUENCY RESPONSE (MFR) FREQUENTLY ASKED QUESTIONS, Jan. 16, 2025, Available: https://www.neso.energy/industry-information/balancing-services/frequency-response-services/mandatory-frequency-response-mfr#Document-library

[54] NESO. Supporting Information. Available: https://www.neso.energy/document/261361/download

[55] T. Li, R. Huang, and L. Chen, et al., "Compression of Uncertain Trajectories in Road Networks," in Proc. 46th Int. Conf. Very Large Data Bases, vol. 13, no. 7, pp. 1050-1063, 2020.

[56] T. Li, L. Chen, CS. Jensen et al., "TRACE: Real-time Compression of Streaming Trajectories in Road Networks," in Proc. 47th Int. Conf. Very Large Data Bases, vol. 13, no. 7, pp. 1175-1187, 2021.